Newton multigrid least-squares FEM for the V-V-P formulation of the Navier-Stokes equations

Masoud Nickaeen, Abderrahim Ouazzi and Stefan Turek

Institut für Angewandte Mathematik (LS III), TU Dortmund
Vogelpothsweg 87, D-44227 Dortmund, Germany
E-mail:{masoud.nickaeen, abderrahim.ouazzi, stefan.turek}@math.tu-dortmund.de

Abstract We solve the V-V-P, vorticity-velocity-pressure, formulation of the stationary incompressible Navier-Stokes equations based on the least-squares finite element method. For the discrete systems, we use a conjugate gradient (CG) solver accelerated with a geometric multigrid preconditioner for the complete system. In addition, we employ a Krylov space smoother inside of the multigrid which allows a parameter-free smoothing. Combining this linear solver with the Newton linearization, we construct a very robust and efficient solver. We use biquadratic finite elements to enhance the mass conservation of the least-squares method for the inflow-outflow problems and to obtain highly accurate results. We demonstrate the advantages of using the higher order finite elements and the grid independent solver behavior through the solution of three stationary laminar flow problems of benchmarking character. The comparisons show excellent agreement between our results and those of the Galerkin mixed finite element method as well as available reference solutions.

Key words: Least-squares FEM, Newton-Multigrid, Conjugate Gradient, Navier-Stokes equations

1 Introduction

The least-squares finite element method (LSFEM) is a numerical method for the solution of partial differential equations. The LSFEM is generally motivated by the desire to recover the advantageous features of Rayleigh-Ritz

methods, as for instance, the choice of the approximation spaces is free from discrete compatibility conditions and the corresponding discrete system is symmetric and positive definite [20].

In this paper, we solve the incompressible Navier-Stokes (NS) equations with the LSFEM. Direct application of the LSFEM to the second-order NS equations requires the use of quite impractical C^1 finite elements [20]. Therefore, we introduce the vorticity as a new variable to recast the NS equations to a first-order system of equations, i.e. the vorticity-velocity-pressure (V-V-P) system. The classical V-V-P formulation has been investigated by many authors, for instance by Bochev [1], Jiang [7] and Bochev and Gungburger [20] and with further modifications by Heys et al. [9, 6, 10]. We study the classical V-V-P system.

As it was mentioned, the resulting LSFEM system is symmetric and positive definite [20]. This permits the use of the conjugate gradient (CG) method and efficient multigrid solvers for the solution of the discrete systems. In order to improve the efficiency of the solution method, the multigrid and the Krylov subspace method, here CG, can be combined with two different strategies. The first strategy is to use the multigrid as a preconditioner for the Krylov method [5]. The advantage of this scheme is that the Krylov method reduces the error in eigenmodes that are not being effectively reduced by multigrid. The second strategy is to employ Krylov methods as multigrid smoother. The Krylov methods appropriately determine the size of the solution updates at each smoothing step [26]. This leads to smoothing sweeps which, in contrast to the standard SOR or Jacobi smoothing, are free from predefined damping parameters.

Heys et al. studied the LSFEM solution of the Stokes equation [5] and the NS equations [8, 9, 10] with an algebraic multigrid preconditioned CG method. A geometric multigrid preconditioned CG solver was used by Ranjan and Reddy [23] for the Spectral/hp LSFEM solution of the NS equations. They demonstrated superior convergence of the multigrid solver compared to the Jacobi preconditioning. More interestingly, Köster [14] and Wobker [26] used preconditioned BiCGStab as smoother in a geometric multigrid method as well as an outer solver around it to solve the Poisson equation with standard Galerkin finite element method. They reported higher numerical stability and lower total costs of the solution process compared to the standalone multigrid or BiCGStab solvers.

We develop a geometric multigrid solver as a preconditioner for the CG (MPCG) iterations to solve the V-V-P system with LSFEM. In addition, we use a CG pre/post-smoother to obtain efficient and parameter-free smoothing sweeps. We demonstrate a robust and grid independent behavior for the solution of different flow problems with both bilinear and biquadratic finite elements.

Despite the advantages of the LSFEM, the lack of local mass conservation of this method is one of its drawbacks. Different strategies have been employed to overcome this deficiency. For very recent techniques and also an overview of the previous efforts we refer to the works of Bochev et al. [17, 18]. One remedy for 2D problems, which is also analyzed in this work, is to use higher order finite elements [13]. Weighting the continuity equation more strongly [11] is another well-known method to recover mass conservation. We show, through the Poiseuille flow and the flow around cylinder problems, that quadratic finite elements satisfy the mass conservation to a great extent without the need to further weight the continuity equation.

Moreover, we show that accurate results can be obtained with V-V-P LSFEM provided that higher order finite elements are used. We demonstrate this with a quantitative analysis of the flow around cylinder and the lid-driven cavity problems.

Therefore, the paper is organized as follows: in the next section we introduce the incompressible NS equations, the continuous and the discrete least-square principles with their properties and the designed LSFEM solver. In the next section, we present the general MPCG solver settings and the detailed results of three incompressible fluid flow problems. Finally, we make a conclusion in the last section.

2 LSFEM for the Navier-Stokes Equations

2.1 Governing Equations

The incompressible NS equations for a stationary flow are given by

$$\begin{cases} \boldsymbol{u}\cdot\nabla\boldsymbol{u}+\nabla p-\nu\triangle\boldsymbol{u}=f & \text{in } \Omega \\ \nabla\cdot\boldsymbol{u}=0 & \text{in } \Omega \\ \boldsymbol{u}=\boldsymbol{g}_D & \text{on } \Gamma_D \\ \boldsymbol{n}\cdot\boldsymbol{\sigma}=\boldsymbol{g}_N & \text{on } \Gamma_N \end{cases} \tag{1}$$

along with the zero mean pressure constraint

$$\int_\Omega p=0 \tag{2}$$

where $\Omega\subset\mathbb{R}^2$ is a bounded domain, p is the normalized pressure $p=P/\rho$, $\nu=\mu/\rho$ is the kinematic viscosity, f is the source term, $\boldsymbol{g}_D$ is the value of the Dirichlet boundary conditions on the Dirichlet boundary Γ_D, $\boldsymbol{g}_N$ is the prescribed traction on the Neumann boundary $\boldsymbol{\Gamma}_N$, $\boldsymbol{n}$ is the outward unit normal on the boundary, $\boldsymbol{\sigma}$ is the stress tensor and $\Gamma=\Gamma_D\cup\Gamma_N$ and

$\Gamma_D \cap \Gamma_N = \emptyset$. The kinematic viscosity and the density of the fluid are assumed to be constant.

The first equation in (1) is the momentum equation where velocities $\boldsymbol{u} = [u\,,\,v]^T$ and pressure p are the unknowns and the second equation represents the continuity equation.

2.2 First-order Systems

The straightforward application of the LSFEM to the second-order NS equations requires C^1 finite elements [20]. To avoid the practical difficulties in the implementation of such FEMs, we first recast the second-order equation to a system of first-order equations. Another important reason for not using the straightforward LSFEM is that the resulting system matrix will be ill-conditioned [19].

Vorticity-Velocity-Pressure Formulation

A common strategy to reformulate the second-order NS equations to an equivalent first-order system is to introduce the vorticity, ω, as a new variable [20]. In two-dimensional problems the vorticity is a scalar and defined as

$$\omega = \nabla \times \boldsymbol{u}. \tag{3}$$

Using the NS equations (1) and the vorticity equation (3) we obtain the first-order Vorticity-Velocity-Pressure (V-V-P) system of equations

$$\begin{cases} \boldsymbol{u} \cdot \nabla \boldsymbol{u} + \nabla p + \nu \nabla \times \omega = f & \text{in } \Omega \\ \nabla \cdot \boldsymbol{u} = 0 & \text{in } \Omega \\ \omega - \nabla \times \boldsymbol{u} = 0 & \text{in } \Omega \\ \boldsymbol{u} = \boldsymbol{g}_D & \text{on } \Gamma_D \\ \boldsymbol{n} \cdot \boldsymbol{\sigma} = \boldsymbol{g}_N & \text{on } \Gamma_N. \end{cases} \tag{4}$$

To obtain the V-V-P system (4), we use the following vector identity

$$\nabla \times \nabla \times \boldsymbol{u} = -\triangle \boldsymbol{u} + \nabla(\nabla \cdot \boldsymbol{u}) \tag{5}$$

and the incompressibility constraint $\nabla \cdot \boldsymbol{u} = 0$. It is easy to show that the first-order V-V-P equations and the NS equations are mutually equivalent [7]. Therefore, based on the analysis provided in the book by Jiang [7] and by Ouazzi [16], we impose no extra boundary conditions for the vorticity.

Linearization of the Convective Terms

The nonlinear convective term, $\boldsymbol{u} \cdot \nabla \boldsymbol{u}$, in the momentum equations needs to be linearized. We linearize the convective term before applying the least-squares technique. Therefore, we use the Newton method to approximate the nonlinear term as follows

$$\boldsymbol{u}^{n+1} \cdot \nabla \boldsymbol{u}^{n+1} \approxeq \boldsymbol{u}^{n} \cdot \nabla \boldsymbol{u}^{n+1} + \boldsymbol{u}^{n+1} \cdot \nabla \boldsymbol{u}^{n} - \boldsymbol{u}^{n} \cdot \nabla \boldsymbol{u}^{n} \tag{6}$$

where superscripts n and $n+1$ refer to the previous and the current nonlinear iterations, respectively.

We terminate the nonlinear iterations when the relative errors, in the Euclidean norm, of the unknowns drop below a certain tolerance ϵ

$$\frac{\left\| U^{n+1} - U^{n} \right\|_2}{\left\| U^{n+1} \right\|_2} < \epsilon \,, \quad U = [\boldsymbol{u}, p, \omega]^T. \tag{7}$$

2.3 Continuous Least-Squares Principles

We define the L^2-norm least-squares energy functionals based on the residuals of the first-order system (4) as follows

$$\begin{aligned} \mathcal{J}(\boldsymbol{v}, q, \xi; f) = \| \boldsymbol{v} \cdot \nabla \boldsymbol{v} + \nabla q + \nu \nabla \times \xi - f \|_0^2 \\ + \alpha \| \nabla \cdot \boldsymbol{v} \|_0^2 + \| \xi - \nabla \times \boldsymbol{v} \|_0^2 \quad \forall (\boldsymbol{v}, q, \xi) \in \boldsymbol{V} \end{aligned} \tag{8}$$

and

$$\begin{aligned} \mathcal{J}_\nu(\boldsymbol{v}, q, \xi; f) = \frac{1}{\nu} \| \boldsymbol{v} \cdot \nabla \boldsymbol{v} + \nabla q + \nu \nabla \times \xi - f \|_0^2 \\ + \alpha \| \nabla \cdot \boldsymbol{v} \|_0^2 + \| \xi - \nabla \times \boldsymbol{v} \|_0^2 \quad \forall (\boldsymbol{v}, q, \xi) \in \boldsymbol{V} \end{aligned} \tag{9}$$

where $\boldsymbol{V}$ is the space of admissible functions

$$\boldsymbol{V} = \left\{ (\boldsymbol{v}, q, \xi) \in \boldsymbol{H}_0^1(\Omega) \times H^1(\Omega) \cap L_0^2(\Omega) \times H^1(\Omega) \right\}. \tag{10}$$

Here, α is a scaling parameter aimed to improve the mass conservation of the LSFEM formulation [11, 21, 22]. The $\mathcal{J}_\nu$ functional, hereafter referred to as the weighted functional, is obtained by scaling the momentum balance equations with the inverse kinematic viscosity.

The minimization problem associated with the least-squares functionals in (8) and (9) is to find $(\boldsymbol{u}, p, \omega) \in \boldsymbol{V}$ such that

$$(\boldsymbol{u}, p, \omega) = \underset{(\boldsymbol{v}, q, \xi) \in \boldsymbol{V}}{\operatorname{argmin}} \, \mathcal{J}(\boldsymbol{v}, q, \xi; f) \tag{11}$$

where the functional $\mathcal{J}$ in equation (11) refers to both the standard and the weighted functionals.

The variational problem based on the optimality condition of the minimization problem (11), considering the approximation in (6), is to find $(\boldsymbol{u}, p, \omega) \in \boldsymbol{V}$ such that

$$\mathcal{A}(\boldsymbol{u}, p, \omega; \boldsymbol{v}, q, \xi) = \mathcal{F}(\boldsymbol{v}, q, \xi) \quad \forall (\boldsymbol{v}, q, \xi) \in \boldsymbol{V} \tag{12}$$

where $\mathcal{A}$ is a bilinear form defined on $\boldsymbol{V} \times \boldsymbol{V} \to \mathbb{R}$

$$\begin{aligned} \mathcal{A}(\boldsymbol{u}, p, \omega; \boldsymbol{v}, q, \xi) := \alpha(\nabla \cdot \boldsymbol{u}, \nabla \cdot \boldsymbol{v}) \\ + (\boldsymbol{u}^n \cdot \nabla \boldsymbol{u} + \boldsymbol{u} \cdot \nabla \boldsymbol{u}^n, \boldsymbol{u}^n \cdot \nabla \boldsymbol{v} + \boldsymbol{v} \cdot \nabla \boldsymbol{u}^n + \nabla q + \nu \nabla \times \xi) \\ + (\nabla p + \nu \nabla \times \omega, \boldsymbol{u}^n \cdot \nabla \boldsymbol{v} + \boldsymbol{v} \cdot \nabla \boldsymbol{u}^n + \nabla q + \nu \nabla \times \xi) \\ + (\omega - \nabla \times \boldsymbol{u}, \xi - \nabla \times \boldsymbol{v}) \end{aligned} \tag{13}$$

and $\mathcal{F}$ is a linear form defined on $\boldsymbol{V} \to \mathbb{R}$

$$\mathcal{F}(\boldsymbol{v}, q, \xi) := (f + \boldsymbol{u}^n \cdot \nabla \boldsymbol{u}^n, \boldsymbol{v} \cdot \nabla \boldsymbol{v} + \nabla q + \nu \nabla \times \xi). \tag{14}$$

For clarity, the bilinear and the linear forms corresponding to the weighted functional (9) are subscripted with ν as follows:

$$\begin{aligned} \mathcal{A}_\nu(\boldsymbol{u}, p, \omega; \boldsymbol{v}, q, \xi) := \alpha(\nabla \cdot \boldsymbol{u}, \nabla \cdot \boldsymbol{v}) \\ + \frac{1}{\nu}(\boldsymbol{u}^n \cdot \nabla \boldsymbol{u} + \boldsymbol{u} \cdot \nabla \boldsymbol{u}^n, \boldsymbol{u}^n \cdot \nabla \boldsymbol{v} + \boldsymbol{v} \cdot \nabla \boldsymbol{u}^n + \nabla q + \nu \nabla \times \xi) \\ + \frac{1}{\nu}(\nabla p + \nu \nabla \times \omega, \boldsymbol{u}^n \cdot \nabla \boldsymbol{v} + \boldsymbol{v} \cdot \nabla \boldsymbol{u}^n + \nabla q + \nu \nabla \times \xi) \\ + (\omega - \nabla \times \boldsymbol{u}, \xi - \nabla \times \boldsymbol{v}) \end{aligned} \tag{15}$$

$$\mathcal{F}_\nu(\boldsymbol{v}, q, \xi) := \frac{1}{\nu}(f + \boldsymbol{u}^n \cdot \nabla \boldsymbol{u}^n, \boldsymbol{v} \cdot \nabla \boldsymbol{v} + \nabla q + \nu \nabla \times \xi) \tag{16}$$

Operator Form of the Problem

To analyze the properties of the least-squares problem, let us write

$$\mathcal{A}(\boldsymbol{u}, p, \omega; \boldsymbol{v}, q, \xi) = \big(\mathsf{L}(\boldsymbol{u}, p, \omega), \mathsf{L}(\boldsymbol{v}, q, \xi)\big) \tag{17}$$

where L is the operator given by

$$\mathsf{L} = \begin{pmatrix} 0 & \nabla & \nu\nabla\times \\ \sqrt{\alpha}\nabla\cdot & 0 & 0 \\ -\nabla\times & 0 & I \end{pmatrix}. \tag{18}$$

Here, I is the identity tensor and ∇, $\nabla\cdot$ and $\nabla\times$ are gradient, divergence and curl operators, respectively. It should be noted that the nonlinear terms are omitted for simplicity.

Restricting to the $C_0^\infty(\Omega)$ functions, we rewrite the bilinear form (17) as

$$\mathcal{A}(\boldsymbol{u},p,\omega;\boldsymbol{v},q,\xi)=\big(\mathbf{L}^*\mathbf{L}(\boldsymbol{u},p,\omega),(\boldsymbol{v},q,\xi)\big) \tag{19}$$

where $\mathbf{L}^*$ is the formal adjoint of $\mathbf{L}$, and the least-squares operator $\mathbf{L}^*\mathbf{L}$ is given by

$$\begin{aligned}\mathbf{L}^*\mathbf{L}&=\begin{pmatrix}0&-\sqrt{\alpha}\nabla&-\nabla\times\\-\nabla\cdot&0&0\\\nu\nabla\times&0&I\end{pmatrix}\begin{pmatrix}0&\nabla&\nu\nabla\times\\\sqrt{\alpha}\nabla\cdot&0&0\\-\nabla\times&0&I\end{pmatrix}\\&=\begin{pmatrix}-\alpha\nabla\nabla\cdot+\nabla\times\nabla\times&0&-\nabla\times\\0&-\nabla\cdot\nabla&0\\-\nabla\times&0&I+\nu^2\nabla\times\nabla\times\end{pmatrix}.\end{aligned} \tag{20}$$

We repeat the same procedure (the derivation is skipped) to obtain the following least-squares operator $\mathbf{L}_\nu^*\mathbf{L}_\nu$ corresponding to the weighted formulation

$$\mathbf{L}_\nu^*\mathbf{L}_\nu=\begin{pmatrix}-\alpha\nabla\nabla\cdot+\nabla\times\nabla\times&0&-\nabla\times\\0&-\frac{1}{\nu}\nabla\cdot\nabla&0\\-\nabla\times&0&I+\nabla\times\nabla\times\end{pmatrix}. \tag{21}$$

The resulting system matrices, from equations (20) and (21), are symmetric and positive definite. So, after discretization, we are able to use the CG method to efficiently solve the system of equations. In addition, both of the least-squares systems are differentially diagonal dominant. This property, combined with the use of higher order finite elements, leads to efficient multigrid solver performance [9]. Our aim is to design an efficient solver which exploits the properties of the least-squares system with respect to both the CG and the multigrid methods. Therefore, we use CG as the main solver and accelerate it with the multigrid preconditioning, which is the previously mentioned MPCG solver.

Also, we use CG as pre/post-smoother which appropriately determines the size of the solution updates at each smoothing step [26]. Therefore, the CG smoothing leads to efficient and particularly parameter-free smoothing sweeps. In addition, we accelerate the smoothing process by using a SSOR preconditioner, which in this context requires no damping parameter in case of symmetric Gauß-Seidel sweeps.

It is worth noting that the possibility of using standard smoothers for the solution of the NS equations is another advantage of the LSFEM over the mixed Galerkin methods that require specially designed smoothers [24].

2.4 Discrete Least-Squares Principle

We introduce the approximation space $\boldsymbol{V_h}$, restrict our variational problem (12) to finite dimensional spaces, and consider the following approximation problem

$$\mathcal{A}_h(\boldsymbol{u}_h, p_h, \omega_h; \boldsymbol{v}_h, q_h, \xi_h) = \mathcal{F}_h(\boldsymbol{v}_h, q_h, \xi_h) \quad \forall (\boldsymbol{v}_h, q_h, \xi_h) \in \boldsymbol{V_h}. \tag{22}$$

Choosing appropriate basis functions for the finite dimensional space $\boldsymbol{V_h}$, we obtain a discrete system of equations for the unknown LSFEM variables, namely $(\boldsymbol{u}_h, p_h, \omega_h)$. Here we use conforming finite elements, therefore we set $\boldsymbol{V_h} \subset \boldsymbol{V}$. In addition, since the well-known LBB condition has not to be satisfied, we use equal-order finite elements in the V-V-P least-squares method.

3 Numerical Results and Discussions

We study three steady state flow problems, i.e. the Poiseuille flow, the flow around cylinder and the lid-driven cavity flow, with both standard LSFEM and weighted LSFEM (W-LSFEM) derived from functionals (8) and (9), respectively. We investigate the performance of the MPCG solver for a wide range of parameters. We compare our results with the results of the mixed finite element method (MFEM) produced by FeatFlow (see *www.featflow.de*), and with available benchmark solutions in the literature.

Moreover, we study the traditional mass conservation problem of the LSFEM through the Poiseuille flow and the flow around cylinder test cases. To investigate the mass conservation, we measure the Global Mass Conservation (GMC) in terms of the fractional change of mass flow rate, defined as

$$\mathrm{GMC} = \frac{\int_{\Gamma_i} \rho\,(\boldsymbol{n}\cdot\boldsymbol{u})\,d\Gamma_i - \int_{\Gamma_o} \rho\,(\boldsymbol{n}\cdot\boldsymbol{u})\,d\Gamma_o}{\int_{\Gamma_i} \rho\,(\boldsymbol{n}\cdot\boldsymbol{u})\,d\Gamma_i} \times 100 \tag{23}$$

where Γ_i is the inflow boundary of the domain and Γ_o is any vertical section between the inflow and the outflow boundaries, including the outflow.

Finally, we perform a quantitative analysis of the lid-driven cavity flow in the laminar regime.

We use the following configurations for all flow simulations unless it is specifically stated:

1. Q_1 (bilinear) or Q_2 (biquadratic) finite elements for all unknowns
2. The MPCG solver for the solution of the linearized system of equations with
   (a) Direct Gaussian elimination (UMFPACK [4]) as coarse-grid solver
   (b) SSOR-preconditioned CG smoother with 4 pre/post-smoothing steps
   (c) F-cycle as the multigrid cycle
   (d) All other components in the multigrid approach, that means intergrid transfer and coarse grid correction, are quite standard and are based on the underlying mesh hierarchy and the properties of the chosen conforming finite elements [24]
3. Relative stopping criterion $\epsilon =$ 1E-6.

3.1 Poiseuille Flow

We study a laminar Poiseuille flow at Reynolds number $Re = 100$ in a square domain of $\Omega = [0,1] \times [0,1]$. The two horizontal solid walls have no-slip boundary conditions. The inflow velocity boundary condition is given by

$$[u, v] = [y(1-y), 0]. \tag{24}$$

The exact pressure solution for this problem is

$$p(x) = 2\nu(L - x) \tag{25}$$

where $L = 1$ is the length of the domain.

Outflow Boundary Conditions

We analyze two different boundary conditions for the outflow boundary. The first one, which comes from the exact solution for the velocity, is to set the same boundary condition as the inflow, i.e. equation (24). This is an essential boundary condition, so it is treated in a strong manner by filtering the system matrix and the right-hand side vector appropriately. The other boundary condition is to prescribe the zero-normal stress on the outflow [12, 13, 23]. The stress tensor for the incompressible fluid is defined as

$$\boldsymbol{\sigma} = -p\mathbf{I} + \nu\nabla\boldsymbol{u} \tag{26}$$

and the outflow boundary condition reads

$$\boldsymbol{\sigma} \cdot \boldsymbol{n} = (-p\mathbf{I} + \nu\nabla\boldsymbol{u}) \cdot \boldsymbol{n} = 0 \quad \text{on} \quad \Gamma_{out} \tag{27}$$

where $\boldsymbol{n}$ is the outward unit vector normal to the outflow boundary Γ_{out}. Considering the fact that we have a vertical outflow section, $\boldsymbol{n} = [1\,,\,0]^T$, equation (27) simplifies to

$$\begin{cases} -p + \nu \dfrac{\partial u}{\partial x} = & 0 \quad \text{on} \quad \Gamma_{out} \\ \nu \dfrac{\partial v}{\partial x} = & 0 \quad \text{on} \quad \Gamma_{out}. \end{cases} \tag{28}$$

We incorporate the boundary conditions in equation (28) into the variational problem (in a weak manner) using the L^2-norm functionals acting on the outflow boundary. Therefore, the energy functional in (8) changes to

$$\begin{aligned} \mathcal{J}_{out}(\boldsymbol{v}, q, \xi; f) = & \left\| \boldsymbol{v} \cdot \nabla \boldsymbol{v} + \nabla q + \nu \nabla \times \xi - f \right\|_0^2 \\ & + \alpha \left\| \nabla \cdot \boldsymbol{v} \right\|_0^2 + \left\| \xi - \nabla \times \boldsymbol{v} \right\|_0^2 \\ & + \left\| (-q\mathbf{I} + \nu \nabla \boldsymbol{v}) \cdot \boldsymbol{n} \right\|_{0,\Gamma_{out}}^2 \quad \forall (\boldsymbol{v}, q, \xi) \in \boldsymbol{V}. \end{aligned} \tag{29}$$

We use a similar treatment to add the boundary terms to the weighted functional (9).

Remark 3.1 *In the case of zero-normal stress boundary conditions, we obtain the exact pressure, equation (25), from the LSFEM simulations. In other words, the zero stress boundary condition helps to make the pressure field unique. However, when we apply Dirichlet velocity boundary conditions on the outflow, we fix the pressure in one point to make the pressure field unique.*

The computational grid contains one quadrilateral element on the first level, level 1, and finer grids are obtained based on the multilevel grid refinement. In the multilevel refinement, every coarse grid is divided into four fine elements by connecting the midpoints of the opposite edges [15]. Then we use the hierarchy of the multilevel grids in our geometric multigrid preconditioner.

Using Q_1 elements, we present the GMC values between the inflow and the different vertical cross-sections of the domain for the LSFEM and the W-LSFEM formulations in Table 1 and Table 2, respectively. The results show that mass conservation improves with mesh refinement and is admittedly satisfied throughout the domain at finer grids. The GMC values are further reduced when a scaling parameter, $\alpha > 1$, is employed at each level. In addition, the results of the Dirichlet outflow boundary condition show slightly better mass conservation compared to those of the zero-normal stress boundary condition. The results of Table 1 and Table 2 show that on coarse grids less mass conservation is achieved with the W-LSFEM in comparison with the standard LSFEM. However, the difference between the two formulations becomes negligible with further grid refinement.

In the case of Q_2 finite elements, the obtained velocity field is exact and the GMC values are zero, up to the iteration error, everywhere in the domain.

This is due to the fact that the Poiseuille flow's parabolic velocity field can be fully represented by the biquadratic finite element. Therefore, we skip here the Q_2 element results.

Table 1. *LSFEM*, absolute values of the GMC in vertical cross-sections of the Poiseuille flow at $Re = 100$ with Q_1 elements

	$\alpha = 1.0$		$\alpha = 10$		$\alpha = 100$	
Lev.	$x = 0.3$	$x = 0.8$	$x = 0.3$	$x = 0.8$	$x = 0.3$	$x = 0.8$
zero-normal stress						
5	1.540063	2.435800	0.520126	0.614301	0.406549	0.416399
6	0.447549	0.722513	0.134901	0.162917	0.101985	0.104672
7	0.138748	0.238623	0.036068	0.046048	0.025626	0.026484
8	0.044002	0.082468	0.009900	0.013754	0.006470	0.006803
Dirichlet boundary condition						
5	0.967960	0.858946	0.457747	0.446324	0.398668	0.397421
6	0.283028	0.250209	0.117297	0.114153	0.099898	0.099585
7	0.082833	0.074349	0.030338	0.029532	0.025029	0.024955
8	0.023621	0.022299	0.007861	0.007731	0.006275	0.006262

Table 2. *W-LSFEM*, absolute values of the GMC in vertical cross-sections of the Poiseuille flow at $Re = 100$ with Q_1 elements

	$\alpha = 1.0$		$\alpha = 10$		$\alpha = 100$	
Lev.	$x = 0.3$	$x = 0.8$	$x = 0.3$	$x = 0.8$	$x = 0.3$	$x = 0.8$
zero-normal stress						
5	2.057919	3.740288	0.627447	0.881192	0.414364	0.438957
6	0.722934	0.140562	0.172234	0.258356	0.105095	0.113889
7	0.215425	0.433627	0.044964	0.069519	0.026494	0.029075
8	0.057796	0.119313	0.011419	0.017906	0.006644	0.007322
Dirichlet boundary condition						
5	1.094678	1.100044	0.490521	0.485411	0.400358	0.399665
6	0.331548	0.348048	0.126444	0.127463	0.100521	0.100554
7	0.091683	0.098458	0.031871	0.032484	0.025170	0.025223
8	0.023839	0.025854	0.007953	0.008146	0.006291	0.006309

3.2 Flow around Cylinder

In this section, we simulate a laminar steady state flow passed a circular cylinder. The geometry of the benchmark configuration consists of a simple channel of length 2.2 and height 0.41. At $[x, y] = [0.2, 0.2]$ a cylinder with diameter $D = 0.1$ is placed. The kinematic viscosity of the fluid is $\nu = 0.001$ and $Re = 20$ which is defined as

$$Re = \frac{U_{mean} D}{\nu} \tag{30}$$

where U_{mean} is the average velocity of the inflow stream and defined as

$$U_{mean} = \frac{2}{3} U_{max}. \tag{31}$$

We refer to [25] and *www.featflow.de/en/benchmarks.html* for further details concerning this benchmark.

Boundary Conditions

The horizontal upper and lower walls and the cylinder have no-slip boundary conditions. The inflow velocity boundary conditions are defined as

$$[u, v] = \left[\frac{1.2y(0.41 - y)}{0.41^2}, 0 \right]. \tag{32}$$

For the outflow boundary, we impose the zero-normal stress boundary condition defined in equation (27).

We present the computational mesh of the coarsest level, level 1, in Figure 1. Correspondingly, Table 3 summarizes the information regarding the number of elements and the number of degrees of freedom.

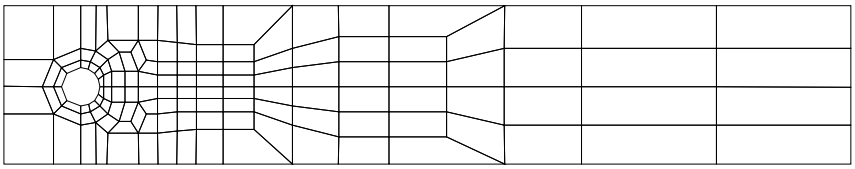

Fig. 1. Flow around cylinder, computational grid of level 1

To investigate the effect of the scaling parameter α, we present the GMC values for two cross-sections (one upstream of the cylinder at $x = 0.05$ and

Table 3. Mesh information for the flow around cylinder problem, the number of elements (NE) and the number of degrees of freedom (NDoF)

		NDoF	
Lev.	NE	Q_1	Q_2
1	130	624	2,288
2	520	2,288	8,736
3	2,080	8,736	34,112
4	8,320	34,112	134,784
5	33,280	134,784	535,808
6	133,120	535,808	2,136,576

the other one on the outflow at $x = 2.2$) in Table 4 and Table 5. The Q_1-element results show that the mass conservation is not well satisfied, even for the fine grids, throughout the domain with $\alpha = 1$. The GMC values reduce with an increase in α. Similar severe mass loss of the LSFEM, when piecewise linear finite elements are used, has been reported by Chang and Nelson [3], Deang and Gunzburger [11] and Bolton and Thatcher [21] for the Stokes flow and by Bolton and Thatcher [22] for the NS equations in the literature.

The Q_2-element results in Table 5 are much superior to those of the Q_1-element and the mass conservation is well satisfied in this case even for the coarsest level with $\alpha = 1$. Similar to the Poiseuille flow, the GMC values become smaller when we increase α, and the difference between the two LSFEM formulations is trivial on the fine grids.

Table 4. GMC in different vertical cross-sections of the flow around cylinder at $Re = 20$ with Q_1 elements

	x-coordinate of the cross-section					
Lev.	0.05	2.2	0.05	2.2	0.05	2.2
LSFEM						
	$\alpha = 1.0$		$\alpha = 10$		$\alpha = 100$	
3	7.602904	47.600894	2.411089	12.180128	1.496185	5.769657
4	3.145125	19.579627	0.830648	3.852176	0.473927	1.618546
5	1.110650	7.160065	0.253329	1.245693	0.128078	0.481929
W-LSFEM						
	$\alpha = 1.0$		$\alpha = 10$		$\alpha = 100$	
3	11.068663	58.389813	3.744287	18.092152	1.836556	7.385963
4	5.236971	30.295098	1.338794	6.673319	0.648462	2.472131
5	1.920968	12.032364	0.386032	2.060374	0.187898	0.777445

Table 5. GMC in different vertical cross-sections of the flow around cylinder at $Re = 20$ with Q_2 elements

	x-coordinate of the cross-section					
Lev.	0.05	2.2	0.05	2.2	0.05	2.2
LSFEM						
	$\alpha = 1.0$		$\alpha = 10$		$\alpha = 100$	
3	0.217743	0.747127	0.098456	0.340778	0.030647	0.111722
4	0.032186	0.107947	0.015427	0.050872	0.009083	0.031029
5	0.004133	0.013817	0.001881	0.006068	0.001416	0.004536
W-LSFEM						
	$\alpha = 1.0$		$\alpha = 10$		$\alpha = 100$	
3	0.424058	1.499480	0.155576	0.542333	0.090863	0.313636
4	0.047289	0.163867	0.017809	0.059399	0.012530	0.041305
5	0.004929	0.016752	0.001962	0.006401	0.001472	0.004738

Next, we analyze the number of nonlinear iterations and the corresponding averaged linear solver (MPCG solver) iterations and present the results for different α in Table 6. We observe a grid-independent convergence behavior and a constant number of iterations with grid refinement at each α, with the optimal number of iterations obtained for $\alpha = 1$. However, the number of the linear solver iterations increases when we depart from $\alpha = 1$. Using Q_2 elements, the required number of iterations for convergence is smaller for the W-LSFEM, showing a better convergence behavior compared with the standard LSFEM.

Table 6. The number of nonlinear iterations and the corresponding averaged number of linear solver iterations for flow around cylinder at $Re = 20$

	LSFEM Q_1			LSFEM Q_2			W-LSFEM Q_1			W-LSFEM Q_2		
	α						α					
Lev.	1.0	10	100	1.0	10	100	1.0	10	100	1.0	10	100
3	8/2	8/2	6/3	10/3	10/6	10/10	8/3	8/3	8/3	7/3	7/4	7/6
4	8/2	8/3	6/4	10/3	10/4	10/9	8/3	8/3	8/5	7/3	7/3	7/7
5	8/2	8/2	8/4	10/2	10/3	10/7	8/3	8/3	8/5	7/3	7/6	8/8

Moreover, we calculate the lift and drag coefficients and the pressure drop across the cylinder. For the definition of these flow parameters one should refer to [25]. We summarize the W-LSFEM results for different α in Table 7. The Q_2-element results are much more accurate than the Q_1-element results, and those pertained to $\alpha = 1$ are in excellent agreement with the benchmark

solutions. Departing from the $\alpha = 1$ case, the accuracy of the flow parameters is degraded especially for the Q_1 elements. The quadratic element results are less sensitive to the α variations compared to the linear element results.

Table 7. *W-LSFEM*, flow parameters in the flow around cylinder at $Re = 20$

	Q_1 elements			Q_2 elements		
Lev.	$\alpha = 1$	$\alpha = 10$	$\alpha = 100$	$\alpha = 1$	$\alpha = 10$	$\alpha = 100$
Drag coefficient C_D						
4	4.2446633	4.9678882	4.4068603	5.5612881	5.5544254	5.4392066
5	5.0579843	5.3925772	5.0770015	5.5771424	5.5754761	5.5551275
6	5.4216095	5.5292391	5.4194334	5.5791512	5.5787593	5.5747834
Lift coefficient C_L						
4	0.0169573	0.0415490	0.107789	0.0103164	0.0105209	0.0115738
5	0.0142112	0.0230143	0.0578331	0.0105818	0.0105999	0.0106819
6	0.0119161	0.0143226	0.0283854	0.0106132	0.0106150	0.0106223
Pressure drop $\triangle p$						
4	0.0834404	0.0964543	0.0769076	0.1170801	0.1170131	0.1151433
5	0.1042858	0.1106489	0.0976744	0.1174629	0.1174541	0.1172354
6	0.1135247	0.1156183	0.1105739	0.1175109	0.1175098	0.1174848
ref. [25]: $C_D = 5.57953523384$, $C_L = 0.010618948146$, $\triangle p = 0.11752016697$						

3.3 Lid-driven Cavity Flow

We simulate the regularized lid-driven cavity flow problem in this section. The flow domain is a unit square which has no-slip boundary conditions on the vertical and lower horizontal walls. The upper wall, the lid, has zero vertical velocity and a horizontal velocity, i.e., the lid velocity. Normally, the lid velocity is taken to be constant which leads to the singularities on the two upper corners of the domain. To remove these singularities, we prescribe a regularized horizontal velocity [2], defined as

$$\boldsymbol{u}_{lid} = [-16x^2(1-x)^2, 0]. \tag{33}$$

We fix the pressure in one point, $p = 0$, in the middle of the lower cavity wall.

In addition to the conventional local velocity profiles, we investigate two other global quantities as defined in [2]. The first one is the kinetic energy defined as

$$E = \frac{1}{2} \|\boldsymbol{u}_h\|^2_{0,\Omega} \tag{34}$$

and the other quantity is the enstrophy defined as follows

$$Z = \frac{1}{2} \|w_h\|^2_{0,\Omega} \tag{35}$$

where $\|\cdot\|_{0,\Omega}$ is the L^2 norm.

Here we use the same computational grid as for the Poiseuille flow problem. We present the percent error of the horizontal velocity through the vertical centerline of the cavity for different Re in Tables 8, 9 and 10. We obtain the percent errors by comparing the W-LSFEM results with the converged reference solutions of the FeatFlow solver on a highly refined grid. At each Re, we use three different computational grids to ensure that grid-independent results are obtained. Results show a very good agreement with the reference solutions at all Re.

Table 8. Percent error of the horizontal velocity through the vertical centerline of the cavity at $Re = 1$, W-LSFEM with Q_2 elements and MFEM with Q_2P_1 elements

	W-LSFEM on Lev.			MFEM
Coord.	7	8	9	ref. value
0.1	0.07	0.01	0.00	4.702885E-02
0.2	0.01	0.00	0.00	8.265610E-02
0.3	0.01	0.00	0.00	1.146949E-01
0.4	0.02	0.00	0.00	1.441905E-01
0.5	0.01	0.00	0.00	1.654724E-01
0.6	0.09	0.01	0.00	1.638459E-01
0.7	0.16	0.05	0.00	1.114928E-01
0.8	0.80	0.27	0.00	-3.903038E-02
0.9	0.22	0.03	0.00	-3.658718E-01

In Table 11, we compare the kinetic energy values of the W-LSFEM with the FeatFlow results for different Re. For the Q_2 elements, we observe excellent convergence with grid refinement and obtain very accurate kinetic energy results for all Re. However, for higher Reynolds numbers, $Re = 1000$, the accurate kinetic energy value is obtained at a relatively finer grid, i.e. level 9. The W-LSFEM results for Q_1 elements are in good agreement with the reference solution only for $Re = 1$. For higher Re, both the asymptotic convergence and the accuracy of the results are affected significantly as compared to the Q_2 element results.

We compare the accuracy of the Q_2 element results of the W-LSFEM with those of Bruneau and Saad [2], obtained with a finite difference method, and also the MFEM reference results for the kinetic energy and the enstrophy. We make this comparison at $Re = 1000$ and summarize the results in Table 12. Both global quantities W and Z converge to the MFEM reference solution

Table 9. Percent error of the horizontal velocity through the vertical centerline of the cavity at $Re = 400$, W-LSFEM with Q_2 elements and MFEM with Q_2P_1 elements

	W-LSFEM on Lev.			MFEM
Coord.	7	8	9	ref. value
0.1	0.75	0.05	0.00	9.447373E-02
0.2	0.50	0.03	0.00	1.817027E-01
0.3	0.11	0.01	0.00	2.335708E-01
0.4	0.30	0.03	0.00	1.967821E-01
0.5	0.68	0.05	0.00	1.040445E-01
0.6	6.35	0.81	0.05	5.466929E-03
0.7	0.68	0.04	0.00	-8.760763E-02
0.8	0.30	0.01	0.00	-1.682347E-01
0.9	0.52	0.06	0.00	-2.365439E-01

Table 10. Percent error of the horizontal velocity through the vertical centerline of the cavity at $Re = 1000$, W-LSFEM with Q_2 elements and MFEM with Q_2P_1 elements

	W-LSFEM on Lev.			MFEM
Coord.	7	8	9	ref. value
0.1	4.57	0.37	0.04	1.787746E-01
0.2	6.10	0.24	0.02	2.767111E-01
0.3	11.35	0.40	0.02	2.128689E-01
0.4	21.37	0.82	0.06	1.275674E-01
0.5	24.31	0.85	0.07	5.190039E-02
0.6	43.34	2.19	0.12	-2.592104E-02
0.7	28.17	1.32	0.09	-1.093997E-01
0.8	18.72	0.89	0.06	-1.985532E-01
0.9	10.37	0.50	0.04	-2.637121E-01

with grid refinement. Also, Table 12 shows that our least-squares solution is more accurate than the solution provided by Bruneau and Saad [2].

4 Conclusion

We used the least-squares FEM to solve the vorticity-velocity-pressure formulation of the incompressible NS equations. Equal order bilinear and biquadratic finite elements are used for the discrete systems. We developed an efficient multigrid-preconditioned CG solver for the solution of the symmetric and positive definite least-squares systems. Also, a preconditioned CG smoother is used inside of the multigrid solver to obtain parameter-free

Table 11. Convergence of the kinetic energy for the regularized cavity problem, comparison between W-LSFEM and MFEM

	W-LSFEM		MFEM	
Lev.	Q_1	Q_2	$\tilde{Q_1}Q_0$	Q_2P_1
$Re = 1$				
7	1.767995E-02	1.862353E-02	1.860621E-02	1.862439E-02
8	1.831566E-02	1.862432E-02	1.861982E-02	1.862438E-02
9	1.853055E-02	1.862438E-02	1.862324E-02	1.862438E-02
$Re = 400$				
7	3.556316E-02	2.133053E-02	2.148649E-02	2.131707E-02
8	3.104720E-02	2.131581E-02	2.136484E-02	2.131547E-02
9	2.394639E-02	2.131537E-02	2.132812E-02	2.131529E-02
$Re = 1000$				
7	1.714473E-02	2.552796E-02	2.409799E-02	2.277778E-02
8	2.962952E-02	2.287704E-02	2.305179E-02	2.276761E-02
9	3.334635E-02	2.277389E-02	2.282649E-02	2.276582E-02

Table 12. Convergence of the kinetic energy E and the enstrophy Z for the regularized cavity problem at $Re = 1000$, comparison between W-LSFEM with Q_2 elements, MFEM with Q_2P_1 elements and the finite difference method in [2]

Method	grid	E	Z
W-LSFEM	64×64	0.025528	4.806740
	128×128	0.022877	4.827331
	256×256	0.022774	4.830225
MFEM	64×64	0.022778	4.829535
	128×128	0.022768	4.830403
	256×256	0.022766	4.830499
Ref. [2]	64×64	0.021564	4.645800
	128×128	0.022315	4.771100
	256×256	0.022542	4.812300
	512×512	0.022607	4.824300

smoothing. We used higher order finite elements to enhance mass conservation of the least-squares method for the inflow-outflow problems. In addition, we have shown that higher order finite elements should be used in order to achieve accurate results with the LSFEM. We studied the accuracy and the performance of the proposed methodology through the solution of the Poiseuille flow, flow around cylinder and the lid-driven cavity problems. Excellent agreement

is obtained between the LSFEM and classical mixed finite element approaches as well as the available benchmark solutions in the literature.

Acknowledgement: This work was supported by the Mercator Research Center Ruhr (MERCUR) grant Pr-2011-0017 and the graduate school of energy efficient production and logistics at TU Dortmund.

References

[1] P. Bochev. Analysis of least-squares finite element methods for the Navier-Stokes equations. *SIAM Journal on Numerical Analysis*, 34(5):1817–1844, 1997.

[2] C.-H. Bruneau and M. Saad. The 2D lid-driven cavity problem revisited. *Computers and Fluids*, 35:326–348, 2006.

[3] C.L. Chang and J.J. Nelson. Least-squares finite element method for the Stokes problem with zero residual of mass conservation. *SIAM J. Numer. Anal.*, 34:480–489, 1997.

[4] T.A. Davis and I.S. Duff. A combined unifrontal/multifrontal method for unsymmetric sparse matrices. *ACM Trans. Math. Softw.*, 25(1):1–20, 1999.

[5] J. J. Heys, T. A. Manteuffel, S. F. McCormick, and L. N. Olson. Algebraic multigrid for higher-order finite elements. *J. Comput. Phys.*, 204(2):520–532, 2005.

[6] J.J. Heys, T.A. Manteuffel, S.F. McCormick, M. Milano, J. Westerdale, and M. Belohlavek. Weighted least-squares finite elements based on particle imaging velocimetry data. *Journal of Computational Physics*, 229(1):107 – 118, 2010.

[7] B.-N Jiang. *The Least-squares finite element method: Theory and applications in computational fluid dynamics and electromagnetics*. Springer-Verlag, 1998.

[8] J.J. Heys, E. Lee, T.A. Manteuffel, and S.F. McCormick. On mass conserving least-squares methods. *SIAM J. Sci. Comput.*, 28:1675–1693, 2006.

[9] J.J. Heys, E. Lee, T.A. Manteuffel, and S.F. McCormick. An alternative least-squares formulation of the Navier-Stokes equations with improved mass conservation. *J. Comput. Phys.*, 226:994–1006, 2007.

[10] J.J. Heys, E. Lee, T.A. Manteuffel, S.F. McCormick, and J.W. Ruge. Enhanced mass conservation in least-squares methods for Navier-Stokes equations. *SIAM J. Sci. Comput.*, 31:2303–2321, 2009.

[11] J.M. Deang and M.D. Gunzburger. Issues related to least-squares finite element methods for the Stokes equations. *SIAM J. Sci. Comput.*, 20:878–906, 1998.

[12] J.P. Pontaza and J.N. Reddy. Spectral/hp least-squares finite element formulation for the Navier-Stokes equations. *J. Comput. Phys.*, 190:523–549, 2003.

[13] J.P. Pontaza and J.N. Reddy. Space-time coupled spectral/hp least-squares finite element formulation for the incompressible Navier-Stokes equations. *J. Comput. Phys.*, 197:418–459, 2004.

[14] M. Köster. *A Hierarchical Flow Solver for Optimisation with PDE Constraints*. PhD thesis, TU Dortmund, 2011.

[15] M. Köster, A. Ouazzi, F. Schieweck, S. Turek, and P. Zajac. New robust nonconforming finite elements of higher order. *Applied Numerical Mathematics*, 62:166–184, 2012.

[16] A. Ouazzi. A mixed formulation of the Stokes equation in terms of (ω, p, u). *Numerical Algorithms*, 21:343–352, 1999.

[17] P. Bochev, J. Lai, and L. Olson. A locally conservative, discontinuous least-squares finite element method for the Stokes equations. *Int. J. Numer. Meth. Fluids*, 68(6):782–804, 2012.

[18] P. Bochev, J. Lai, and L. Olson. A non-conforming least-squares finite element method for incompressible fluid flow problems. *Int. J. Numer. Meth. Fluids*, 00:1–19, 2012.

[19] P. Bochev and M. Gunzburger. Least-squares finite element methods. In *Proceedings of the International Congress of Mathematicians (ICM)*, Madrid, 2006. Plenary Lectures.

[20] P. Bochev and M. Gunzburger. *Least-squares finite element methods*. Springer, 2009.

[21] P. Bolton and R.W. Thatcher. On mass conservation in least-squares methods. *J. Comput. Phys.*, 203:287–304, 2005.

[22] P. Bolton and R.W. Thatcher. A least-squares finite element method for the Navier-Stokes equations. *J. Comput. Phys.*, 213:174–183, 2006.

[23] R. Ranjan and J.N. Reddy. On multigrid methods for the solution of least-squares finite element models for viscous flows. *International Journal of Computational Fluid Dynamics*, 26:45–65, 2012.

[24] S. Turek. *Efficient Solvers for Incompressible Flow Problems: An Algorithmic and Computational Approach*. Springer, Berlin, 1999.

[25] S. Turek and M. Schäfer. Benchmark computations of laminar flow around cylinder. In E.H. Hirschel, editor, *Flow Simulation with High-Performance Computers II*, volume 52 of *Notes on Numerical Fluid Mechanics*, pages 547–566. Vieweg, 1996.

[26] H. Wobker. *Efficient Multilevel Solvers and High Performance Computing Techniques for the Finite Element Simulation of Large-Scale Elasticity Problems*. PhD thesis, TU Dortmund, 2010.